CHAPTER VII
ANALYSIS

This chapter is organized as following. Section 7.1 studies sources of background. Section 7.2 describes subtraction of the non-J/ψ background. Resolutions of the reconstructed kinematical variables are presented in Section 7.3. Section 7.4 compares main features of the real candidates and the Monte Carlo events. In Section 7.5, acceptance is studied using different Monte Carlo event samples, different selection procedures, and with different background subtraction methods. The electroproduction cross section is then determined. In Section 7.6, the photoproduction cross section is derived from the electroproduction cross section. Section 7.7 discusses systematic errors. Section 7.8 is a summary of the cross section measurement.

7.1 Background

There are three types of background to the elastic $J/\psi \to e^+e^-$ process. The first is due to genuine J/ψ produced from inelastic production where hadrons escape detection through the beampipe. The dominant process here is due to diffractive dissociation of the proton as shown in Figure 1(c) in Chapter I. The second type is due to genuine e^+e^- pair produced from Bethe-Heitler process $\gamma p \to e^+e^-p$(Figure 38). The third type is due to hadrons h^+h^-(mostly pions) misidentified as electrons. The amount of genuine J/ψ background from other production processes can be estimated from Monte Carlo simulations of these processes. The amount of genuine e^+e^- background from Bethe-Heitler process is also estimated from Monte Carlo simulation of this process. Background contributions from h^+h^- misidentification can be estimated from the real data as will be described below.

7.1.1 Pion pair background

Conceptually, $J/\psi \to e^+e^-$ candidates can be selected in two steps. In the first step, events leaving exactly two oppositely charged particles x^+x^-(x stands for any unspecified particle) inside the main detector are selected without applying particle identification but with all the kinematic requirements such as the range of track momentum, track rapidity and $\sqrt{s_{\gamma p}}$. In the second step, x^+x^- pairs are passed through the electron filter. The electron filter has nearly 100 percent acceptance for genuine e^+e^- pairs and a misidentification probability $P_{hh\to ee}$ for those h^+h^- events which have passed the first step selection. If the electron filter rejects $N_{\rm rej}$ events in a given bin, then the estimated number of the remaining h^+h^- events in that bin is

$$N_{hh} = N_{\rm rej}\frac{P_{hh\to ee}}{1-P_{hh\to ee}} \tag{63}$$

assuming no e^+e^- event is rejected.† $P_{hh\to ee} = P_{h\to e}P_{h\to e}$ can be estimated from a sample of pions in the same low energy range(there is no correlation between $P_{h\to e}$ of different tracks since in the diffractive x^+x^- sample the two clusters are completely separated in the calorimeter as a result of the kinematic constraints). In our experiment, the electron identification had been partly done in the online J/ψ triggers and partly done in the offline J/ψ DST filter. The two-step method is still applicable if a more stringent electron filter is used in the second step.

We re-selected a sample of J/ψ events from the 1993 MINIDST data in two steps. In the first step, a sample of diffractive x^+x^- was selected with all the

† If this is not the case, the estimated number of rejected e^+e^- must be subtracted from $N_{\rm rej}$ before applying Eq. (63)

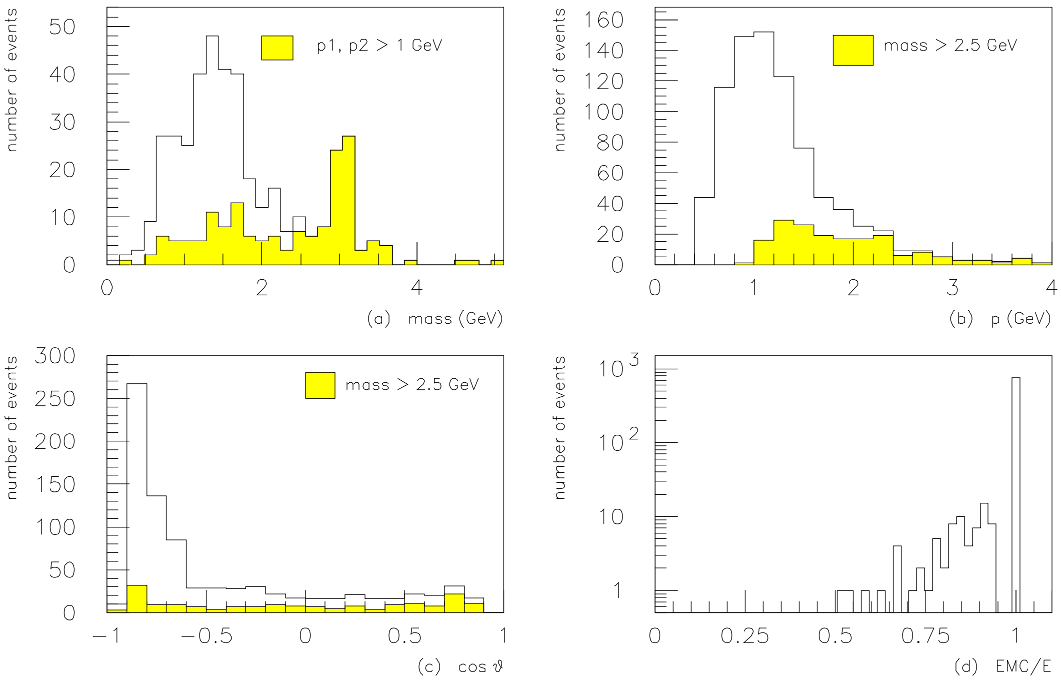

Figure 34: Profile of the diffractive x^+x^- sample. (a) J/ψ mass peak(2.85-3.25 GeV) stands out clearly. Shaded area corresponds to events with both tracks of momentum greater than 1 GeV. (b) Histogram of the track momentum. Almost all of the events of interest (mass greater than 2.5 GeV) have track momentum between 1 and 3 GeV. (c) Polar angular distribution of the tracks. Tracks in events of large invariant mass distribute much more isotropically. (d) In 90 percent of the events, $E_{EMC} > 0.9E_{cluster}$ for both clusters, as a result of the TLT $J/\psi toee$ requirement.

requirements of the standard diffractive $J/\psi \to e^+e^-$ selection except for the electron identification, plus the requirement that the event must be accepted by the TLT $J/\psi \to e^+e^-$ trigger, since this trigger accepted most of the J/ψ events and made no explicit electron identification. This sample contained 414 events. Figure 34 shows the features of this sample. The J/ψ mass peak stands out very clearly in Figure 34(a). It is interesting to note that most of the h^+h^- events have been rejected before being tested by an electron filter. Therefore the large electron to pion ratio in the J/ψ mass peak region does not reflect the ratio of $P_{ee\to ee}$ to $P_{hh\to ee}$ of the electron filter.

Since $P_{h\to e}$, the probability for a pion to be misidentified as an electron, cannot be determined from this small sample of diffractive x^+x^-, a selection of a large sample of pions from inelastic(multi-track) data is needed. However, in order for $P_{h\to e}$ determined from the multi-track pion sample to be applicable to the diffractive two-track x^+x^- sample, the multi-track pion sample must be selected in a biased way similar to that of the two-track x^+x^- sample, in view of the electron filter. Now let us discuss what requirements in the x^+x^- selection may affect $P_{h\to e}$.

The electron filter is based on the calorimeter response to the incident particle. The incident particle is described by its track momentum p and polar angle θ(the detector is symmetric in azimuthal angle ϕ). The calorimeter response is described by the cluster energy in the EMC section(E_{EMC}) and the HAC section(E_{HAC}), and the transverse size of the cluster $R_{cluster}$.†

Separation of electrons and hadrons is based on the following parameters: (1) $\frac{E_{EMC}}{E_{EMC}+E_{HAC}}$; (2) $\frac{E_{EMC}}{p}$; (3) $R_{cluster}$. In the limited range of p between 1 to 3 GeV, p independent cuts on E_{EMC} and $R_{cluster}$ can be used. Figure 35 shows the distributions of the above parameters for electrons and pions, where electrons are from Monte Carlo simulated J/ψ events and "pions" were picked from the real data of multi-track(more than three tracks) events.

The first requirement on an electron filter is that it enhances the product $\rho\sqrt{n}$, where ρ is the purity and n is the number of events. For practical convenience, we add a second requirement that $P_{e\to e}$ be nearly 100% and $P_{h\to e}$ is nearly uniform in track p and θ. The electron filter used in this analysis is quite close to this ideal. Then the kinematic requirements on track p_t and η(pseudo-rapidity) are irrelevant. The number of tracks in an event is also irrelevant since $P_{h\to e}$ is not affected by the presence of other tracks in the event. However, for two-track diffractive events, the TLT $J/\psi \to ee$ trigger tends to select events with cluster energy contained

† $R_{cluster}$ is measured by the r.m.s.(σ) of the cell coordinate(using the coordinate along the narrower side of the cell) weighted by the cell energy.

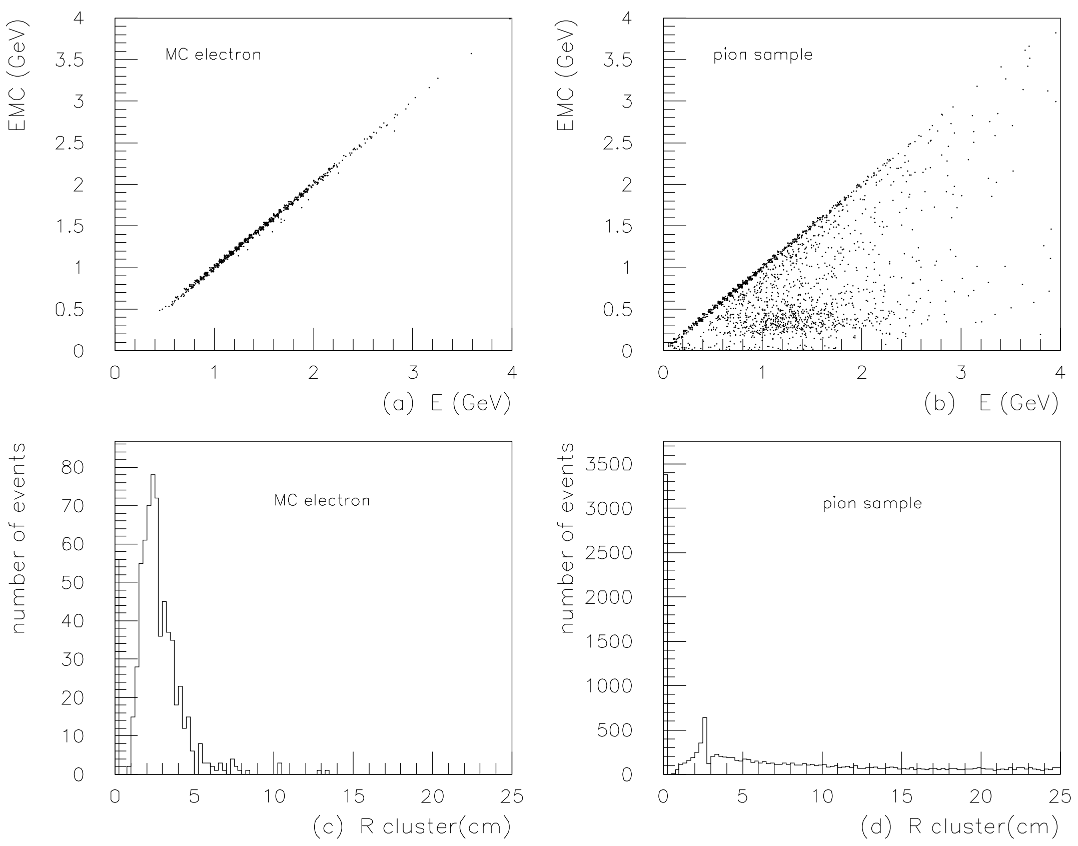

Figure 35: Comparison of the calorimeter response to e and π. (a) $E_{EMC} \approx E_{cluster}$ for electrons. (b) $E_{EMC} < E_{cluster}$ for 60% of the low energy pions. (c) $R_{cluster} < 10$ cm for electrons. (d) Some pions have $R_{cluster} > 10$ cm. $R_{cluster}$ is set to zero cm for single cell clusters.

in the EMC section. This effect can be simulated by adding a requirement that $\frac{E_{EMC}}{E_{EMC}+E_{HAC}} > 0.9$ in both diffractive x^+x^- sample and pion samples. Track p range should also be the same in x^+x^- sample and pion samples.

According to above discussions, pions were selected by requiring track momentum p be between 1 to 3GeV (see the shaded area of Figure 34(b)) and more than 90% of the cluster energy be contained in the EMC section. It was also required that track multiplicity be no less than 4. In a multi-track event, a track is most likely due to a charged pion, and electron contamination is not a concern.

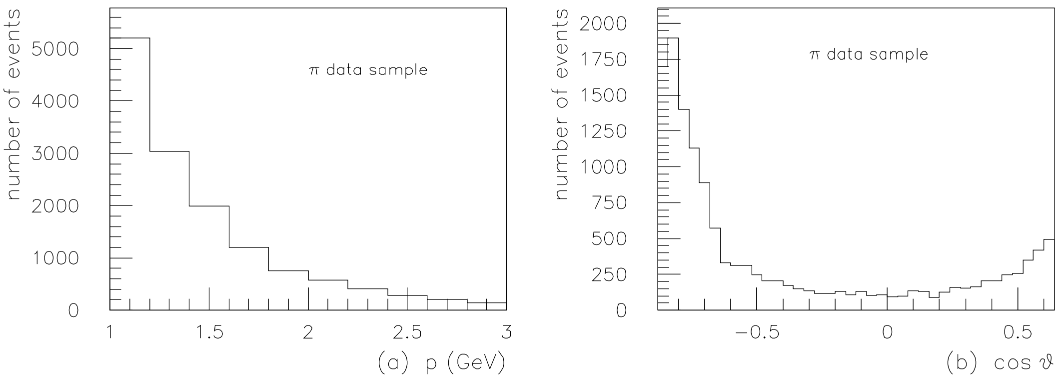

Figure 36: Profile of the pion sample. The track momentum and angle are in the same range as those in the x^+x^- sample.

In multi-track events, mismatching between tracks and clusters presents a problem. This was solved by requiring the track multiplicity be no more than 10, and by adding a more stringent requirement on the track-cluster matching quality factor for both x^+x^- sample and pion samples. If an event contained more than one pion tracks, the track with largest θ was chosen. Histograms in Figure 36 show the kinematic range of these pions. The calorimeter response to the pions has been shown in Figure 35. Most of the selected pions were in the rear direction. This is because out of all pion tracks in an event, the track with the largest polar angle was always selected. This choice was motivated by the angular distribution of the tracks in the diffractive x^+x^- events, but is inconsequential.

The electron filter requires

(1) $E_{EMC} > 0.9E_{cluster}$

(2) $E_{EMC} > 0.5$ GeV

(3) $R_{cluster} < 10$ cm (the width of cell is 5 cm)

$R_{cluster}$ is not constrained if the cluster spans across the gap between two calorimeters. This electron filter is calibrated by the $J/\psi \to e^+e^-$ Monte Carlo events and the real pion data. The results are $P_{e\to e} = 0.98$, $P_{ee\to ee} = 0.95$(agrees with

$P_{ee\to ee} = P^2_{e\to e}$), $P_{h\to e} = 0.70$ with $P_{hh\to ee} = P^2_{h\to e} = 0.50$. Figure 37(a) and (b) show that $P_{e\to e}$ and $P_{h\to e}$ are nearly uniform in track p and θ. Note that $P_{h\to e} = 0.70$ is a *conditional probability*, with the condition $E_{EMC} > 0.9E_{cluster}$.

Table 17: pion background study

selection	remaining events	mass=2.85-3.25 GeV
diffractive x^+x^-	414	58
pion cuts	113	50
electron filter	91	44

The diffractive x^+x^- events were first passed through the pion sample selection criteria which requires that the track p be between 1 to 3 GeV, $E_{EMC}/E_{cluster} > 0.9$ and the track-cluster matching quality factor be greater than 0.98 for both tracks. Then the remaining events were tested by the electron filter. The results are summarized by Table 17 and shown in Figure 37.

Since the electron filter's acceptance to genuine e^+e^- and h^+h^- is estimated to be 0.95 and 0.50 respectively, and 6 out of 44 events are rejected, we may conclude that 4 of the 6 rejected events are likely to be h^+h^- and the other 2 rejected events are likely to be e^+e^- events. Then the number of remaining h^+h^- events under the mass peak estimated from Eq. (63) is 4 ± 2, with statistical fluctuation. This result was found to be stable with variations of the electron filter criteria.

From this study we conclude that the final selection of the elastic $J/\psi \to e^+e^-$ contains about $9\pm 5\%$(4 ± 2 out of 44 events) background events from misidentified pion pairs in the mass peak region 2.85-3.25GeV, and about $30 \pm 9\%$ (14 ± 4 out of 47 events) outside the mass peak region.

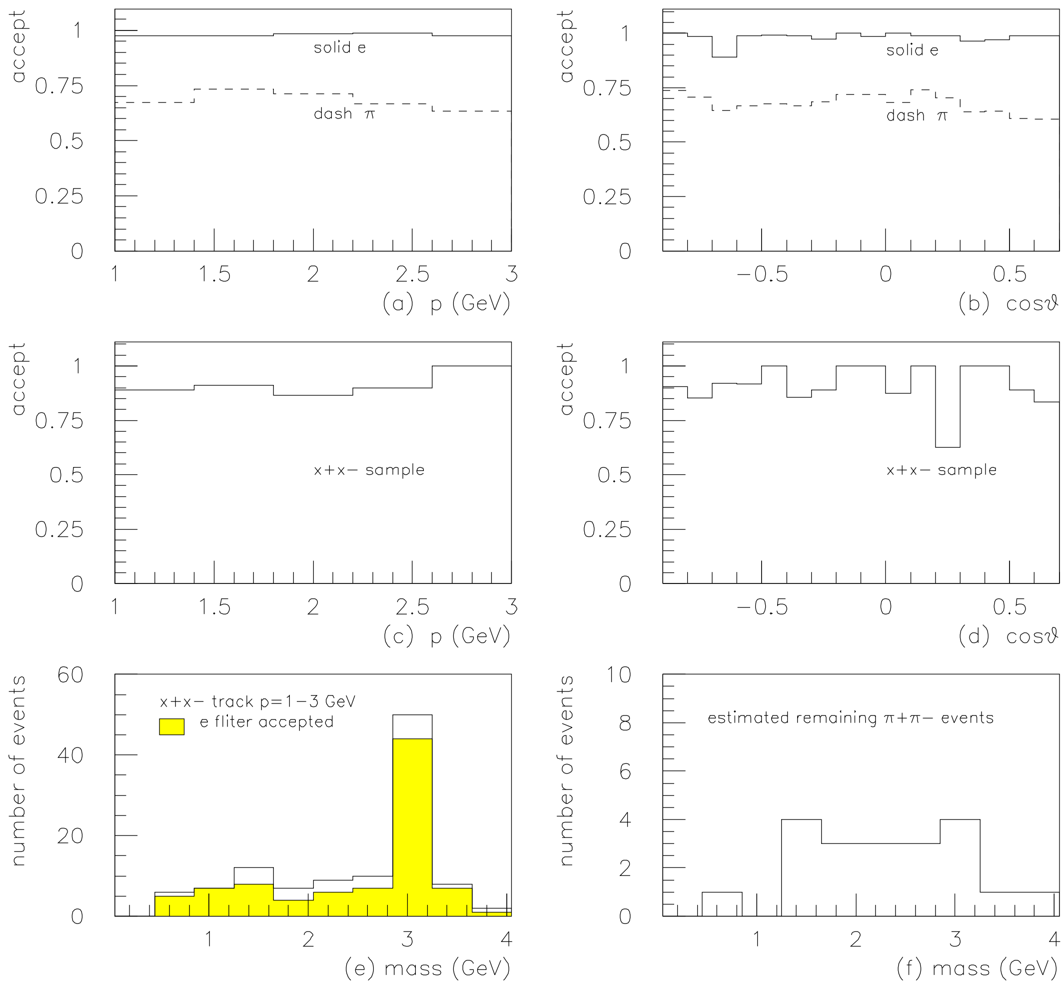

Figure 37: Estimation of the pion background. (a) and (b) show that the electron filter is close to ideal. $P_{e \to e}$ is near 100%(0.98). $P_{h \to e}$ is not sensitive to p and θ of the pion track. (c) and (d) show the electron filter's acceptance to the x^+x^- events. (e) Invariant mass distribution before and after the electron filter. (f) Estimated number of remaining h^+h^- events in each invariant mass bin.

7.1.2 Bethe-Heitler e^+e^- background

Figure 38 shows elastic and inelastic Bethe-Heitler processes of e^+e^- pair production. Both elastic and inelastic Bethe-Heitler e^+e^- events were generated using

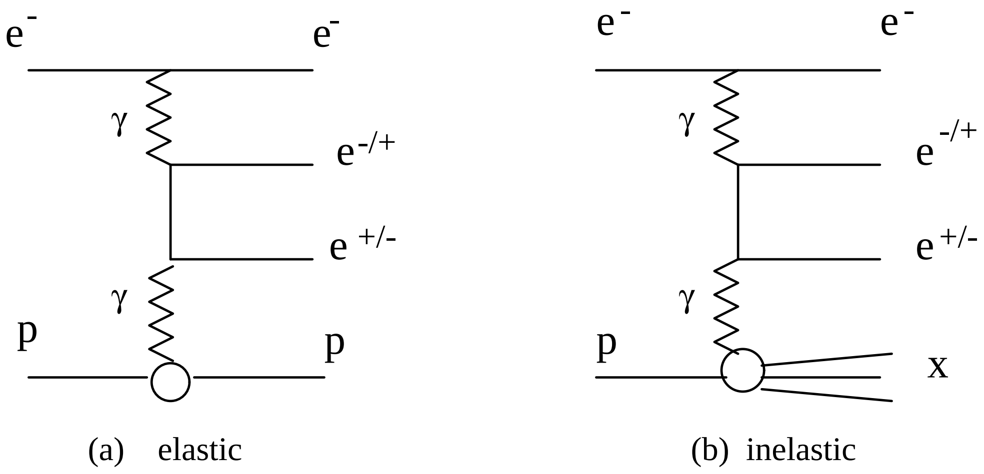

Figure 38: Feynman diagrams of Bethe-Heitler e^+e^- pair production. (a) Diagrams of elastic process. Note that the virtual photon from the beam e^- may couple to either e^+ or e^-, corresponding to two distinguishable diagrams. (b) Diagrams of the inelastic process where the proton is broken.

the LPAIR program.[75] In LPAIR, p-γ-p vertex is taken to be the proton form factor for elastic process and the proton structure function for inelastic process. The following detector cuts have been applied to both tracks of e^+ and e^- in generating these events:

(1) $p > 1.0\text{GeV}$

(2) $p_t > 0.5\text{GeV}$

(3) $5^\circ < \theta < 175^\circ$

Theoretical cross sections are 817.9$\pm$6.4pb for the elastic process and 338.9$\pm$0.8pb for the inelastic process. These MC events were passed through the ZEUS detector and trigger simulations and the standard diffractive $J/\psi \to e^+e^-$ selection. MC events were normalized to the data luminosity 488nb^{-1} by assigning an event weight $w = \mathcal{L}_{data}\sigma^{(theory)}/N^{(MC)}$, where $N^{(MC)}$ is the number of generated events. It is found that 23 ± 5 (statistical fluctuation) events have passed all selection criteria.

7.1.3 Proton diffractive background

This background is discussed in detail in Ref. 79. Here we explain the method and result briefly. By removing the diffractive(CAL-quiet) requirement in the elastic J/ψ candidate selection, 20% more events were selected in the mass region 2.85-3.25GeV. By visually scanning these events, it was determined that about 5% were most likely due to the proton diffractive process(the other 15% were most likely events with $Q^2 > 4\mathrm{GeV}^2$ so that the beam electron enter the RCAL). This procedure, event selection with and without the CAL-quiet requirement, was also applied to the Monte Carlo diffractive J/ψ generated using PYTHIA.[76,77] It was thus determined that the proton diffractive process accounts for $15 \pm 7(\mathrm{stat.}) \pm 7(\mathrm{theo.})\%$ of the J/ψ cross section. The statistical error is due to the small number of real data events in the diffractive tail. The theoretical error is due to the uncertainty in the mass distribution of the hadrons X. The mass distribution was parameterized as $d\sigma/dM_x^2 \sim M_x^{-n}$ (with n varying between 2 and 3).

7.2 Fitting of the invariant mass spectrum

The final sample of elastic $J/\psi \to e^+e^-$ events contains non-J/ψ background as can be seen from the invariant mass spectrum. The discussion in Section 7.1 helps to understand the nature of the background. Subtraction of the continuum background is more easily and reliably done either by the maximum likelihood fitting method, or by the naive baseline subtraction method.

In the maximum likelihood(ML) method, the invariant mass spectrum is fitted with assumed functions $f^{(\mathrm{signal})}$ and $f^{(\mathrm{noise})}$, with the number of signal events as one of the free parameters. Monte Carlo studies show that the signal distribution is well described by a Gaussian term $g(m; m_{J/\psi}, \sigma)$ and a Bremsstrahlung tail $b(m; m_{J/\psi}, \sigma)$ which is a convolution of a Gaussian function and a Bremsstrahlung factor.[78]